Determination of Anisotropic Optical Constants and Surface Coverage of Molecular Films Using Polarized Visible ATR Spectroscopy. Application to Adsorbed Cytochrome *c* Films

Anne F. Runge,[†] Nicole C. Rasmussen,[†] S. Scott Saavedra,[†] and Sergio B. Mendes*[,†,‡]

Department of Chemistry, and Optical Sciences Center, University of Arizona, Tucson, Arizona 85721

Received: September 20, 2004; In Final Form: October 22, 2004

This article describes a method to determine the anisotropic optical constants and surface coverage of molecular films using polarized attenuated total reflectance (ATR) absorbance measurements. We have extended the transfer-matrix formalism to describe birefringent and dichroic films in ATR geometries and have combined it with an iterative numerical procedure to determine the anisotropic values of both the real (*n*) and imaginary (*k*) parts of the complex refractive index of the film under investigation. Anisotropic values of the imaginary part of the refractive index (*k*) allow for the determination of the surface coverage and one order parameter of the film. To illustrate this approach, we have used cytochrome *c* (cyt *c*) protein films adsorbed to glass and indium tin oxide (ITO) surfaces. Experimental results show that cyt *c* films on these surfaces, which were formed under identical conditions, have significant differences in their surface coverages (11.2 ± 0.4 pmol/cm^2 on glass and 21.7 ± 0.9 pmol/cm^2 on ITO); however, their order parameters $\langle\cos^2\theta\rangle$ are similar (0.30 ± 0.02 on glass and 0.36 ± 0.04 on ITO).

1. Introduction

Attenuated total reflectance (ATR) spectroscopy is a useful technique for studies of adsorbed molecular films because of its enhanced sensitivity relative to direct transmission measurements. In addition, the probing electric field is spatially confined near the surface, which imparts a high selectivity for sampling surface events with negligible interference from bulk dissolved components. The use of a polarized light beam in ATR absorbance measurements allows for the determination of the transition dipole strength along each lab coordinate axis and the associated optical anisotropy of a film under investigation. Since Harrick's pioneering work,[1] molecular dichroism calculations with polarized ATR spectroscopy are traditionally performed by first determining the electric field intensities along each Cartesian direction and then using the respective measured absorbance values to solve for the transition dipole projection along each Cartesian direction. When dealing with either a two-phase system or a three-phase system in which the center layer can be approximated as an extremely thin film (on the order of a few nanometers for visible light) surrounded by two semi-infinite media, the expressions for the electric fields are readily available[1] and the approach is straightforward. To calculate the electric field for more complex geometries several researchers have employed a rigorous electromagnetic wave approach using a transfer-matrix, which relates the tangential components of the electromagnetic field from one interface to another interface across the intervening layer. The matrix elements depend on the optical constants and thickness of the layer. This formalism was first developed by Abelès[2] in 1950 and since then has been a key analytical tool for designing multilayer stacks for optical interference filters; the approach is mainly known to the chemistry community through the work of Hansen.[3] However, most transfer-matrix calculations of the electric field in ATR configurations have ignored the extinction coefficient (imaginary part of the complex refractive index) of the absorbing layer by implicitly assuming its value to be zero. A few works[4,5] have included the extinction coefficient in the matrix calculation, although these only considered the simplest case of an isotropic extinction coefficient.

Polarized ATR is routinely employed for studies of dichroic layers, which mathematically should be represented by an anisotropic extinction coefficient that allows for a different value along each Cartesian direction. An anisotropic extinction coefficient can affect the values one calculates for the electric field, which will ultimately affect the molecular anisotropy one determines for the dichroic layer. In addition to this limitation, transfer-matrix calculations presented in the literature for ATR applications[4,5] have focused mainly on the determination of the Cartesian components of the electric field, which are essentially used as auxiliary variables for subsequent calculations of either (a) the polarized absorbance using anisotropic optical constants determined (or known) by other means or (b) the anisotropic optical constants from polarized ATR data. In configurations where the thickness of the absorbing layer cannot be neglected, the electric field is no longer constant across this layer, and an average needs to be evaluated to obtain accurate absorbance results, which makes the overall calculation cumbersome as already pointed out by Axelsen.[5] An approach that overcomes these difficulties was provided by Buffeteau et al.[6] who reported a transfer-matrix formalism and numerical procedure in which the anisotropic optical constants are calculated directly without explicit determination of the electric fields (although they are rigorously considered in the calculations). However, due to their choice of spectroscopic techniques (normal incidence transmission and reflection−absorption infrared spectroscopy (RAIRS)), the anisotropic optical constants are decoupled in each measurement: normal incidence transmittance only involves an electric field component either along *x* or *y*, and RAIRS only involves

* To whom correspondence should be addressed. Voice: (520) 621-6340. Fax: (520) 621-8407. E-mail: sergiom@email.arizona.edu.
[†] Department of Chemistry, University of Arizona.
[‡] Optical Sciences Center, University of Arizona.

10.1021/jp045727e CCC: $30.25
Published on Web 12/07/2004

the *z*-component; therefore the conventional transfer-matrix formalism developed for isotropic media is sufficient to describe their experiments. In an ATR experiment, because the TM polarization contains electric field components in both the *x* and *z* directions, the optical constants in both directions are simultaneously present in the experimental results, and the isotropic transfer-matrix expressions cannot be applied.

Following the seminal work of Berreman[7] and Yeh,[8] Parikh and Allara[9] and Yamamoto and Ishida[10] have outlined a general transfer-matrix formalism to describe the interaction of polarized light with a stratified multilayer stack composed of anisotropic layers. In this work, we apply this formalism to specifically describe polarized ATR experiments involving an anisotropic molecular layer, and show a procedure to recover the anisotropic optical constants, the molecular surface coverage, and one order parameter from the ATR data. First, we use the transfer-matrix formalism to calculate polarized reflectance (*R*) values, instead of the conventional approach of determining electric field values. Once reflectance is known, polarized ATR absorbance (*A*) values are determined through the following expression: $A = -\log_{10}(R^r)$, where *r* is the number of reflections at the interface between the molecular layer and the ATR guiding element. This approach circumvents an explicit determination of the electric field, which is implicitly and rigorously included in the transfer-matrix analysis. Variations in the electric field within an absorbing layer are automatically considered when calculating reflectance (and consequently also absorbance), and the approach avoids the need to calculate electric field intensities at every point across an absorbing film for an accurate absorbance determination. Next, we extend the expressions of the transfer-matrix approach to allow the molecular layers to have both a dichroic extinction coefficient (imaginary part of the complex refractive index) and a birefringent refractive index (real part of the complex refractive index). Last, a numerical procedure is established to determine the anisotropic optical constants, which then allow calculation of the molecular surface coverage and one order parameter.

To demonstrate this method, we have applied it to adsorbed films of cytochrome *c* (cyt *c*) on glass and indium tin oxide (ITO) surfaces. For biosensors based on the activity of surface immobilized proteins, a major question is how to control the structure and orientation of these proteins, which presumably affect sensor performance.[11,12] Cyt *c* is often used as a model protein to address these questions and immobilized cyt *c* films have been studied using a variety of surface sensitive spectroscopic techniques.[13−17] Glass and ITO are both negatively charged surfaces with heterogeneous surface chemistries. ITO is a semiconductor which can directly oxidize and reduce adsorbed cyt *c*, depending on the potential applied to the surface. The advantage of optically determining the surface coverage of an adsorbed film on an electrode surface is that all molecules in the film are probed, not only the electroactive portion accessible through voltammetry[18−20] and other electrochemical methods.[21] For electrochemically based sensors, both the total surface coverage and the electroactive surface coverage of the protein film are important quantities to measure. In this paper, we use identical conditions (buffer, bulk protein concentration) to form adsorbed cyt *c* protein films on two different substrates, and demonstrate how this method is used to determine the optical constants of the films as well as their surface coverage and order parameters.

2. Theory

In the ATR configuration shown in Figure 1 with our choice of coordinate system, a light beam propagates in the *x*-*z* plane

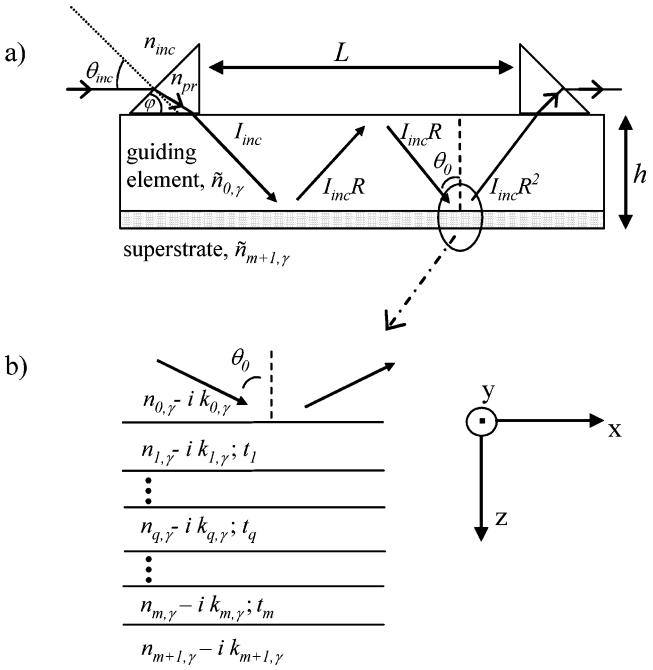

Figure 1. (a) ATR configuration showing the path of the light beam as it is incoupled, reflected down the ATR substrate, and outcoupled. (b) Expanded view of the multilayer structure showing our coordinate system where the *x*−*y* plane is the sample plane and light is propagating in the *x*−*z* plane.

through a transparent guiding medium (here called medium 0) and impinges on a stratified assembly composed of *m* arbitrary layers ($m \geq 1$) and a semi-infinite superstrate (medium $m + 1$). The superstrate must have a refractive index (n_{m+1}) lower than that of the guiding medium (refractive index, n_0) and the angle, θ_0, in medium 0 must be greater than the critical angle, $\theta_{crit} = \sin^{-1}(n_{m+1}/n_0)$, to prevent power from flowing into the superstrate medium, although an exponentially decaying, evanescent field is still present in this medium. The analytical ATR signal is measured after the beam has been reflected several times along the length of the guiding element. The absorbance signal, *A*, can be calculated by the following expression

$$A = -\log_{10}\left(\frac{I}{I_{inc}}\right) = -\log_{10}\left(\frac{I_{inc}R^r}{I_{inc}}\right) = -r\log_{10}(R) \quad (1)$$

if the reflectance, *R*, for a single reflection and the number of reflections, *r*, are determined. The number of reflections can be easily determined from geometrical considerations and is given by[22]

$$r = \frac{L\sqrt{n_0^2 - N^2}}{2hN} \quad (2)$$

where *h* is the thickness of the guiding element, *L* is the distance between the in- and out-coupling prisms, n_0 is defined above, and *N* is the effective refractive index (also called Snell's invariant, $N = n_0 \sin\theta_0$). *N* is experimentally determined by the incoupling conditions of the propagating beam into the guiding element[23]

$$N = n_0 \sin\theta_0 = n_{inc}\sin\theta_{inc}\cos\varphi + (n_{pr}^2 - n_{inc}^2\sin^2\theta_{inc})^{1/2}\sin\varphi \quad (3)$$

as shown in Figure 1, where θ_{inc} is the angle between the prism

normal and the incident beam, φ and n_{pr} are the prism base angle and refractive index, respectively, and n_{inc} is the refractive index of the medium (usually air) outside the prism.

Focusing on ATR applications involving anisotropic layers, we allow for the refractive index of any layer to have different values along each Cartesian direction. The real part of the refractive index is then described in general by three numbers n_x, n_y, n_z; similarly, the imaginary part of the refractive index is described by k_x, k_y, k_z. The complex anisotropic refractive index of any layer is written as

$$\tilde{n}_{\alpha,\gamma} = n_{\alpha,\gamma} - ik_{\alpha,\gamma} \tag{4}$$

where $\alpha = 0, 1, 2, ..., m-1, m, m+1$ specifies a particular medium and $\gamma = x, y, z$ defines a particular Cartesian axis.

To extend the isotropic transfer-matrix approach to include optically anisotropic films as described by eq 4, Horowitz and Mendes,[24] following Berreman's formalism,[7] have shown that it is sufficient to generalize the expressions for the phase, β, and admittance, η, used in the transfer-matrix (defined below). For the transverse electric (TE) polarization, these terms are given by

$$\beta_\alpha = \frac{2\pi}{\lambda} t_\alpha \sqrt{\tilde{n}_{\alpha,y}^{\,2} - N^2}, \quad \alpha = 1, ..., m \tag{5}$$

$$\eta_\alpha = \sqrt{\tilde{n}_{\alpha,y}^{\,2} - N^2}, \quad \alpha = 0,1,..., m,m+1 \tag{6}$$

and for the transverse magnetic (TM) polarization, they are written as

$$\beta_\alpha = \frac{2\pi}{\lambda} t_\alpha \sqrt{\frac{\tilde{n}_{\alpha,x}^{\,2}}{\tilde{n}_{\alpha,z}^{\,2}}(\tilde{n}_{\alpha,z}^{\,2} - N^2)}, \quad \alpha = 1, ..., m \tag{7}$$

$$\eta_\alpha = \frac{\tilde{n}_{\alpha,x}\tilde{n}_{\alpha,z}}{\sqrt{\tilde{n}_{\alpha,z}^{\,2} - N^2}}, \quad \alpha = 0, 1, ..., m, m+1 \tag{8}$$

where λ is the light beam wavelength measured in a vacuum and t_α is the thickness of layer α. With these expressions, the reflectance, R, of a light beam incident from a transparent medium ($k_{0,\gamma} = 0$) and impinging onto a stratified stack (which can include anisotropic and absorbing media) can be expressed for both polarizations in the usual format:[25]

$$R = \left|\frac{\eta_0 B - C}{\eta_0 B + C}\right|^2 \tag{9}$$

where B and C are calculated using the matrix relation

$$\begin{pmatrix} B \\ C \end{pmatrix} \equiv \begin{pmatrix} U \\ V \end{pmatrix}_{(0,1)} = M_1 \times M_2 \times ... \times M_m \begin{pmatrix} U \\ V \end{pmatrix}_{(m,m+1)} \tag{10}$$

and the transfer-matrix M_α is defined by

$$M_\alpha \equiv \begin{pmatrix} \cos\beta_\alpha & \frac{i}{\eta_\alpha}\sin\beta_\alpha \\ i\eta_\alpha \sin\beta_\alpha & \cos\beta_\alpha \end{pmatrix} \tag{11}$$

The transfer-matrix M relates the values of the tangential components of the electric (U) and magnetic (V) fields at the two interfaces that bound a particular layer. In our notation, the subscript (0, 1) represents the boundary between the guiding medium (0) and the first layer (1), and the subscript (m, $m+1$) represents the boundary between the last layer (m) and the superstrate ($m+1$). The transfer-matrix M_α uses the optical constants of layer α ($n_{\alpha,\gamma}$, $k_{\alpha,\gamma}$, and t_α, with $\gamma = x, y, z$) to relate the tangential electromagnetic fields at the interfaces ($\alpha - 1$, α) and (α, $\alpha + 1$).

For the TE polarization, the tangential components of the electromagnetic field, U and V, are given by

$$\begin{pmatrix} U \\ V \end{pmatrix} = \begin{pmatrix} E_y \\ -H_x\sqrt{\mu_{vac}/\epsilon_{vac}} \end{pmatrix} \tag{12}$$

and for the TM case are described by

$$\begin{pmatrix} U \\ V \end{pmatrix} = \begin{pmatrix} E_x \\ H_y\sqrt{\mu_{vac}/\epsilon_{vac}} \end{pmatrix} \tag{13}$$

where the vacuum permittivity, ϵ_{vac}, and permeability, μ_{vac}, were used to provide the same physical dimension (units) to both vector components U and V, which simplifies the notation of the admittance and transfer-matrix. Finally, the calculation with eq 10 can be performed by noting that, at the last interface, the electric and magnetic field components can be related by

$$\begin{pmatrix} U \\ V \end{pmatrix}_{(m,m+1)} = \begin{pmatrix} 1 \\ \eta_{m+1} \end{pmatrix} \tag{14}$$

since only a forward propagating wave is present in the superstrate.

Once the Snell's invariant (N), optical constants ($n_{\alpha,\gamma}$, $k_{\alpha,\gamma}$), and thicknesses (t_α) of the stratified stack are known, eqs 5−14 provide a straightforward approach for the calculation of polarized reflectance results. It is important to note that the definition of the complex refractive index with a minus sign in eq 4 for the imaginary part was dictated by a particular choice of the time-harmonic description of the electromagnetic wave, $e^{i(\omega t - \beta z)}$, as already discussed by others.[3,25] Consistency with this choice also requires that, among the possible mathematical solutions for eqs 5 and 7 involving the square root of complex numbers, the physically acceptable solution will satisfy the condition $\mathrm{Im}\{\beta\} \leq 0$ as the light beam power should exponentially decay, not grow, as it propagates in an absorbing medium.

To summarize to this point, we have outlined a method to calculate reflectance, R, of a light beam probing a stratified stack of anisotropic layers, which are described by eq 4. For ATR experiments, the transfer-matrix formalism above combined with eqs 1 and 2 provides a direct path for calculating polarized absorbance values, A_{TE} and A_{TM}. This method avoids an explicit calculation of auxiliary variables such as the Cartesian components of the electric field across an absorbing layer, although these fields are rigorously considered in the entire calculation and variations of the electric field strength across any absorbing layer are automatically considered. In addition, the transfer-matrix formalism includes the anisotropic optical constants of any layer in the stratified stack; therefore, the effects of birefringent and dichroic layers on the electromagnetic fields, and ultimately on the absorbance results, are fully and rigorously accounted for in this analysis.

The transfer-matrix formalism above shows that once the optical constants of a stratified stack are known, absorbance calculations are straightforward. However, we typically face the inverse problem, where absorbance data are collected and determination of the anisotropic optical constants of a particular layer is desired. Although an explicit solution relating the optical constants of the layer to the polarized ATR data is not possible (or would be extremely cumbersome), a simple numerical procedure can solve the inverse problem. In this procedure, the

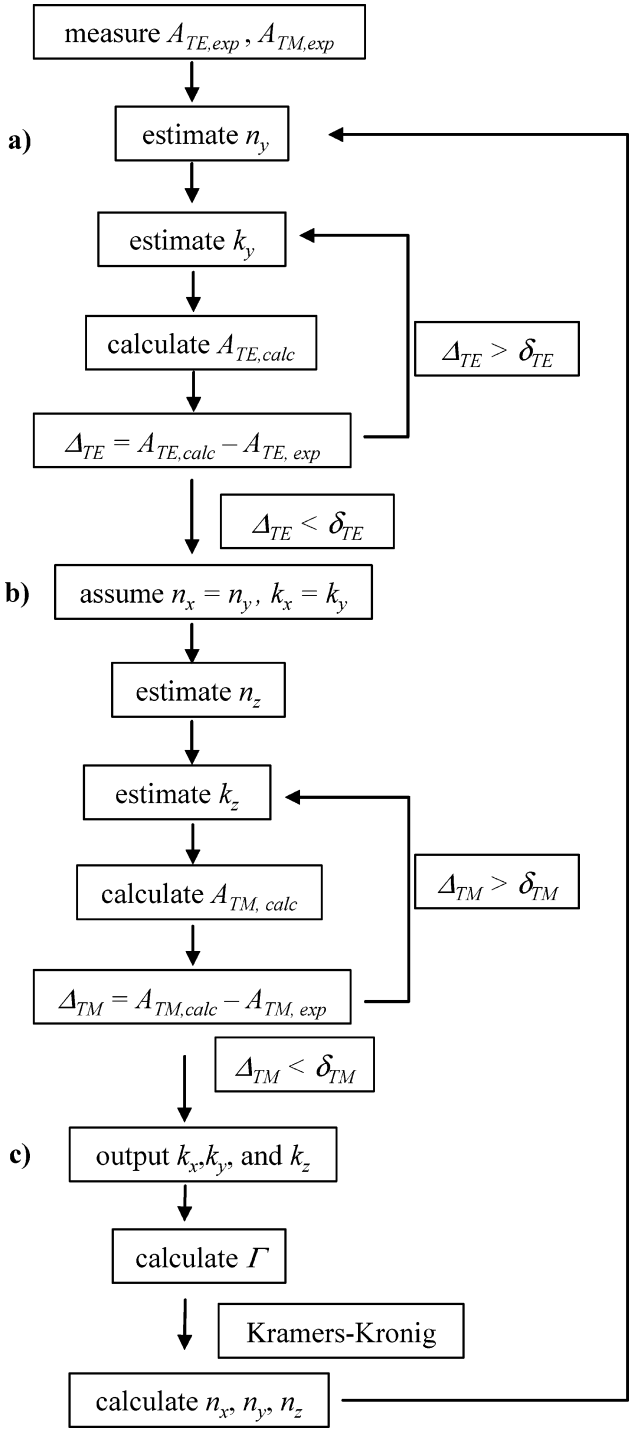

Figure 2. Flowchart for iteration process to determine n_x, n_y, n_z, k_x, k_y, k_z, and Γ for layer q from measured values of A_{TE}, A_{TM}.

value for the complex refractive index of the absorbing layer (an adsorbed cyt *c* film in the present work, here called layer *q*) is varied in an iterative manner to match the calculated and experimental absorbance values. If the stratified stack is composed of multiple layers, the optical constants and thickness of the other layers must be known (or determined by other techniques). The iteration process is summarized in a flowchart shown in Figure 2 (for simplicity, the subscript *q* is dropped; all optical constants and surface coverages are for layer *q*).

(a) TE polarized absorbance data are considered first because they involve only the *y*-component of the refractive index given in eqs 5 and 6; the real part of the refractive index of the protein film along the *y*-axis (n_y) is initially estimated, and then the value for k_y is iteratively varied to make the difference between calculated and experimental absorbances, $\Delta_{TE} = |A_{TE,calc} - A_{TE,\,exp}|$, less than (typically 10 times smaller) the precision in the experimental measurement (δ_{TE}).

(b) Second, we consider the TM absorbance data for which the calculations involve both *x* and *z* components of the refractive index, as described in eqs 7 and 8. However, for many types of molecular films (including the adsorbed cyt *c* films examined here), we can assume in-plane symmetry for the optical constants (the molecules are randomly oriented in the sample plane), which allow us to write $n_x = n_y$ and $k_x = k_y$. Next, a value for the real portion of the refractive index along the *z*-axis (n_z) is estimated and a value for k_z that minimizes the difference in TM absorbance, $\Delta_{TM} = |A_{TM,calc} - A_{TM,\,exp}|$, is iteratively determined.

(c) Once the imaginary parts of the refractive index along each Cartesian axis are determined, then the surface coverage (Γ) can be calculated through the following relation:[22]

$$\Gamma = \frac{4\pi(k_x + k_y + k_z)t_q}{3\epsilon\lambda \ln(10)} \tag{15}$$

Here ϵ is the molar absorptivity of the dissolved molecule (i.e., measured in solution) and t_q is the thickness of the layer. Layer *q* is formed by solute molecules that may be dispersed in a solvent matrix (in this study, cyt *c* in an aqueous solution). The thickness of the layer is a function of the dimensions, conformation, and packing geometry of the solute molecule. The real portion of the refractive index of this layer depends on the solute and solvent concentration in the layer. For the adsorbed cyt *c* films examined here, we used the surface coverage obtained from eq 15, the molar absorptivity of cyt *c* measured over a broad spectral range, and Kramers−Kronig (KK) relations (discussed in the following section) to refine the initial estimate for the real part of the refractive index along each Cartesian axis, n_γ.

Once refined n_γ values are determined, the previously described routine (steps a−c) is repeated to generate refined values of k_γ and Γ, which are used to further refine values of n_γ. This loop is repeated until it reaches a numerical precision that is better than the experimental precision determined by the uncertainties in the absorbance measurements. Typically this process converged in just a few loops (3−5), even when we intentionally provided initial estimates of n_γ that were significantly different from the expected final result.

According to KK relations,[26] if the imaginary part of the refractive index (extinction coefficient) is known over the entire frequency range, the real part of the refractive index can be calculated. These quantities are related through the complex optical susceptibility. For a film with an extinction coefficient of k_q and formed by molecules with a susceptibility $\chi = \chi' + i\chi''$ dispersed in a transparent solvent of refractive index n_{m+1}, we can write[26]

$$-\chi'(\nu) = 2n_{m+1}k_q(\nu) = 2n_{m+1}\frac{\lambda \ln(10)\,\epsilon(\nu)\Gamma}{4\pi t_q} \tag{16}$$

for any frequency, ν. Then the real part of the susceptibility, χ', can be calculated using a KK relation[26]

$$\chi'(\upsilon_0) = \frac{2}{\pi}\int_0^\infty \frac{\chi''(\nu)\,\nu}{\nu^2 - \upsilon_0^2}\,d\nu \tag{17}$$

which allows the determination of the real part of the refractive

index (in the case of a weakly absorbing medium, $\chi'' \ll 1$):[26]

$$n_q(\nu_0) = n_{m+1} + \frac{\chi'(\nu_0)}{2n_{m+1}} \tag{18}$$

Since the spectral information on the molar absorptivity $\epsilon(\nu)$, and therefore on $\chi(\nu)$, is limited to a finite range (for instance, from ν_1 to ν_2), eq 17 is calculated by

$$\chi'(\upsilon_0) = \frac{2}{\pi}\int_{\nu_1}^{\nu_2} \frac{-\chi_\gamma''(\nu)\,\nu}{\nu^2 - \upsilon_0^2}\,d\nu + f\frac{\Gamma}{t_q} \tag{19}$$

where the second term is dependent on the concentration of the solute molecule in the layer of interest. This corrects for background absorption bands outside the integral that affect the real component of the optical susceptibility. The coefficient f can be experimentally determined by measuring the dependence of the refractive index on the concentration of the solute molecule dissolved in the solvent matrix.

Finally we note that, since k_γ is in general anisotropic for an adsorbed molecular film, the molar absorptivity $\epsilon(\nu)$ in eq 16 is replaced by

$$\epsilon_\gamma(\nu) = 3\epsilon(\nu)\frac{k_\gamma(\nu_0)}{k_x(\nu_0) + k_y(\nu_0) + k_z(\nu_0)} \tag{20}$$

and eqs 16, 19, and 18 are calculated for each Cartesian direction γ to determine the anisotropic real part of the refractive index (n_γ).

Once the anisotropic optical constants have been determined, an order parameter, $\langle\cos^2\theta\rangle$, can then be calculated for the layer of interest using the dichroic values of the imaginary part of the complex refractive index: k_x, k_y, and k_z.[22,27] In the case of a linear dipole it is given by

$$\langle\cos^2\theta\rangle = \frac{k_z}{k_x + k_y + k_z} \tag{21}$$

where θ is the angle between the dipole and the z axis, and in the case of a circular dipole it is given by

$$\langle\cos^2\theta\rangle = 1 - \frac{2k_z}{k_x + k_y + k_z} \tag{22}$$

where θ is the angle between the normal to the dipole plane and the z axis.

3. Experimental Section

Cytochrome *c*. Horse heart cytochrome *c* (Sigma) was purified on a cation exchange column as described in previous studies.[18,28] Ten micromolar solutions of ferricytochrome *c* in 10 mM phosphate buffer (pH 7) were used to prepare all protein films. Deionized (DI) water (18 MΩ) was obtained from a Barnstead Nanopure apparatus and was used throughout.

Substrates. Glass microscope slides (Gold Seal Products #3010) were cleaned in a Chromerge (Manostat) bath at 60 °C for 1 h and rinsed thoroughly with DI water before use. Indium tin oxide (ITO) films on soda lime glass (Colorado Concept Coatings) with a sheet resistance of approximately 20 ohms-per-square**,** and a root-mean-square (rms) surface roughness of 1−2 nm (determined using atomic force microscopy on scan areas of 1 μm^2) were used throughout. The ITO substrates were cleaned by scrubbing with a 2% Triton-X solution for 1 min, and then sonicating for 10 min each in 2% Triton-X, water, and ethanol,[29] followed by low-temperature air plasma cleaning (Harrick model PDC-3XG) for 15 min at 30 W. Before use, ITO substrates were soaked for 12−48 h in 10 mM phosphate buffer, pH 7. Wet chemical etching of ITO was accomplished by soaking the ITO coated substrates in a 6 M HCl/0.2 M $FeCl_3$ solution for 5 min.[30,31]

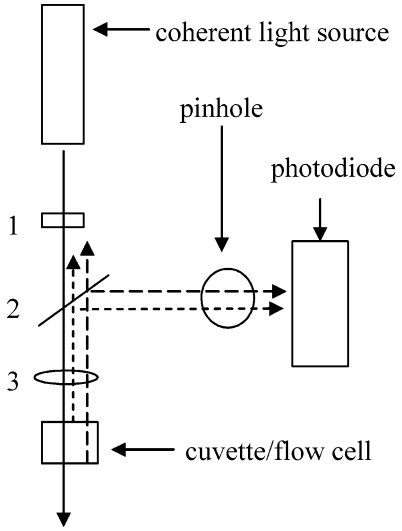

Figure 3. Interferometer setup: (1) lens to expand beam; (2) beam splitter (glass slide); (3) iris. The solid line is the incident beam and the dashed lines are the beams reflected from the front and back glass/air interfaces of the cuvette.

ATR Measurements. The attenuated total reflectance instrument has been described previously.[32] Briefly, collimated light from a Xe lamp was coupled into the glass slide (or ITO-coated glass slide) with a fused silica prism. The collimated beam was about 1 mm in diameter. The beam was totally internally reflected down the length of the slide mounted in a liquid flow cell (about 10−12 reflections over $L = 50$ mm, $h = 1.0$ mm) before being outcoupled by another prism and detected with a photomultiplier through a 413 nm band-pass filter (15 nm fwhm; Edmund Optics R43-054). The outcoupled beam was chopped at 1700 Hz and lock-in amplification was used to increase the signal-to-noise ratio. The blank transmission was measured with 10 mM phosphate buffer in the flow cell. A cyt *c* solution was then injected into the flow cell and equilibrated with the surface for 15 min before flushing the cell with 10 mL of 10 mM buffer. After the bulk protein solution was removed, the transmission was measured. For this instrumental setup, the molar absorptivity (ϵ) of cyt *c* was calculated to be 80388 M^{-1} cm^{-1} based on the published molar absorptivities of ferricyt *c*[33] and the band-pass filter transmission profile.

Refractive Index of Dissolved Protein at Different Concentrations. For the implementation of KK relations, the dependence of the refractive index of dissolved cyt *c* on protein concentration was measured at one wavelength (633 nm). The measurement was performed using an interferometric technique[34,35] with the optical setup shown in Figure 3. A He−Ne laser with an expanded beam was used as a coherent light source; reflection from the cuvette walls provided the two beams needed to generate the interference pattern (one beam probing the sample solution and the other was used as a reference). The beams were redirected with a beam splitter, spatially filtered by a 400-μm pinhole, monitored with a photodiode detector, and recorded with Labview software. Counting interference fringes as the protein concentration was varied allowed the refractive index dependence on the protein concentration to be determined.

a)

$n_0 = 1.51, k_0 = 0$ (glass)

$n_{1,\gamma} - i\,k_{1,\gamma}; t_1 = 3$ nm (adsorbed cytochrome *c* layer)

$n_2 = 1.3425, k_2 = 0$ (buffer)

b)

$n_0 = 1.51, k_0 = 0$ (glass)

$n_1 = 1.91, k_1 = 0; t_1 = 67$ nm (ITO)

$n_{2,\gamma} - i\,k_{2,\gamma}; t_2 = 3$ nm (adsorbed cytochrome *c* layer)

$n_3 = 1.3425, k_3 = 0$ (buffer)

Figure 4. (a) Multilayer structure for cyt *c* films on glass substrates. (b) Multilayer structure for cyt *c* films on ITO substrates.

4. Results and Discussion

Optical Constants and Layer Thicknesses. For cyt *c* adsorbed on a glass slide, the stratified system (Figure 4a) is composed of glass (medium $\alpha = 0$), the protein film ($\alpha = 1$), and buffer solution ($\alpha = 2$). For the ATR experiment with cyt *c* adsorbed on an ITO-coated glass slide (see Figure 4b), there are four media to consider: glass ($\alpha = 0$), ITO ($\alpha = 1$), the protein film ($\alpha = 2$), and buffer solution ($\alpha = 3$). In these configurations, the only anisotropic and absorbing medium is the cyt *c* film; the other media are assumed to be isotropic and transparent ($k = 0$). While ITO does absorb some visible light (e.g., $k \sim 0.01-0.02$ at 450 nm),[36] this is taken into account by first measuring the blank transmission for the ITO slide before cyt *c* is adsorbed. As long as k_{ITO} is much less than n_{ITO}, this absorbance will not significantly perturb the electromagnetic fields in this system. As described in the Theory section, to calculate A_{TE} and A_{TM} the following parameters must be known: n_{glass}, n_{ITO}, t_{ITO}, $t_{cyt\,c}$, n_{buffer}, and N. The bare glass slides and the glass underlying the ITO film were both assumed to have a refractive index of $n_{glass} = 1.51$. The ITO thickness, t_{ITO}, and refractive index, n_{ITO}, at the wavelength of interest (413 nm) were obtained by curve fitting the optical transmittance of the ITO-coated slide measured at normal incidence in a conventional UV−vis spectrophotometer (400−900 nm).[25] Values of $t_{ITO} = 67 \pm 2$ nm and $n_{ITO} = 2.088$ were determined. The ITO thickness was also verified by etching the ITO coating[30,31] on one section of the slide. The step height from the etched section to an unetched section of the slide was measured using tapping mode AFM, which gave thicknesses in the range of 65−70 nm. In all calculations, a thickness of 67 nm was used. A thickness of $t_{cyt\,c} = 3$ nm was assumed for the protein film based on the dimensions of cyt *c*.[37] The refractive index of the bulk aqueous phase, n_{buffer}, was calculated to be 1.3425 at 413.5 nm from literature results.[38] For the calculation of the effective refractive index, N (eq 3), our incoupling conditions were as follows: $n_{inc} = 1.00$, $n_{pr} = 1.46$, $\varphi = 45°$, and θ_{inc} was measured for each set of data.

Kramers—Kronig Calculations for Refractive Index of Protein Films. For the application of KK relations, the dependence of the cyt *c* refractive index on its concentration in an aqueous solution was determined with our interferometric setup. For cyt *c* concentrations in the range from 0 to 0.0013 g/cm^3 prepared in 10 mM phosphate buffer, we obtained a value of $dn/dc = 0.17 \pm 0.03$ cm^3/g, which agrees reasonably well with a value of 0.1854 cm^3/g measured by Kekicheff et al.[39] over a much broader range of cyt *c* concentrations (0.25 to 0.80 g/cm^3). In addition to the dn/dc slope, the molar absorptivity of ferricyt *c* must be known over a wide frequency range for application of KK relations. Molar absorptivity values of ferricyt *c* between 200 and 950 nm (at 1 nm intervals) were obtained from both the literature[33] and by measuring the UV−vis spectrum of cyt *c* over this entire frequency range. These results (dn/dc and ϵ values) allowed us to determined a value of $f = 5.26$ M^{-1} for use in eq 19. Figure 5a shows a typical refractive index profile for cyt *c* films on glass along with molar absorptivity values, ϵ_γ, calculated from eq 20. The values for the refractive index are lower and show less dispersion than the corresponding films on ITO (see Figure 5b). This difference reflects the smaller volume fraction occupied by cyt *c* molecules in layer $t_{cyt\,c}$ (the assumed thickness of which was held constant at 3 nm). In other words, we have represented the protein film as a 3 nm layer (based on the dimensions of cyt *c*[37]) regardless of surface coverage (up to one monolayer), so that n_γ varies with the concentration of protein in the layer. This, in our opinion, is a more physically reasonable model than one in which $t_{cyt\,c}$ is the average of the film thickness over areas of the surface with and without adsorbed protein (in that model, $t_{cyt\,c}$ would be less than 3 nm for a submonolayer film).

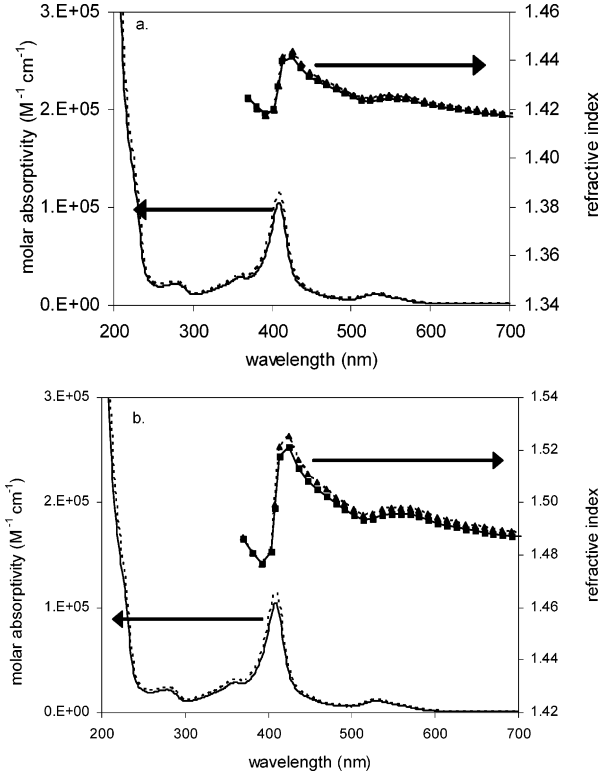

Figure 5. Visible absorbance spectra of cyt *c* and refractive index profile for adsorbed films on glass (a) and ITO (b). Molar absorptivity of cyt *c* (calculated using eq 20) in the plane of the substrate (ϵ_x, ϵ_y; solid line), out of the plane (ϵ_z; dashed line), refractive index profile of cyt *c* calculated at discrete wavelengths in the plane (n_x,n_y; solid lines with squares at calculated points), and out of the plane (n_z; dashed line with triangles at calculated points).

Anisotropic Optical Constants and Surface Coverage. As an illustration of the calculation procedure, Table 1 shows one set of experimental data collected for an adsorbed cyt *c* film on an ITO-coated glass substrate with values for θ_{inc} (which is used to calculate N), A_{TE}, A_{TM}, and r. Also shown are the initial estimates for n_γ and the calculated values for n_x, k_x, n_y, k_y, n_z, k_z, and Γ at each step of the iteration process previously described. As seen, the process converges quite rapidly despite an intentional estimate for n_γ that was significantly different than the recovered value. In addition, we observe that the in-plane (x and y) and out-of-plane components (z) of the complex refractive index converged to similar values ($n_x = n_y \cong n_z$, k_x

TABLE 1: Iteration Cycle for One Set of Experimental Data (cyt *c* on ITO)

Experimental Data					
substrate	θ_{inc}	N	A_{TE}	A_{TM}	r
ITO	37.00 ± 0.02[a]	1.366 ± 0.006[b]	0.031 ± 0.004[a]	0.08 ± 0.01[a]	11

Results					
	$n_x = n_y$	n_z	$k_x = k_y$	k_z	Γ (pmol/cm^2)
initial	1.33[c]	1.70[c]	0.053	0.063	27.5
1	1.570	1.579	0.043	0.048	21.8
2	1.523	1.528	0.046	0.045	22.3
3	1.5 ± 0.2	1.53 ± 0.07	0.046 ± 0.006	0.045 ± 0.006	22 ± 2

[a] Standard deviation based on three measurements. [b] Propagated error. [c] Initial estimates of variables.

TABLE 2: Optical Constants, Surface Coverage, and One Order Parameter for Cyt *c* Films on Glass and ITO

	glass[a]	ITO[b]
$n_x = n_y$	1.44 ± 0.06	1.5 ± 0.1
$k_x = k_y$	0.022 ± 0.001	0.045 ± 0.004
n_z	1.44 ± 0.03	1.52 ± 0.03
k_z	0.024 ± 0.002	0.042 ± 0.002
Γ (pmol/cm^2)	11.2 ± 0.4	21.7 ± 0.9
$\langle\cos^2\theta\rangle$	0.30 ± 0.02	0.36 ± 0.04

[a] Three separate samples. [b] Five separate samples.

$= k_y \cong k_z$). This means that these particular cyt *c* films have no significant birefringence or dichroism.

Table 2 lists the experimental results for the optical constants and surface coverage of cyt *c* on glass and ITO substrates. The surface coverage obtained on glass substrates is 11.2 ± 0.4 pmol/cm^2, or about half a monolayer of cyt *c* based on the dimensions of the protein molecule (a close packed monolayer would be 22 pmol/cm^2).[14] Previous work reported a surface coverage of cyt *c* adsorbed on a hydrophilic glass substrate of 29 pmol/cm^2, which was measured by a protein desorption assay.[40] In addition to the different analytical approaches used in these measurements, we also attribute the different experimental results to the higher dissolved protein concentration used in the cited work (35 μM) vs that used here (10 μM). In a recently published study by Cheng et al.,[13] the surface coverage of cyt *c* on a glass substrate was determined using ATR spectroscopy to be a full monolayer (23 pmol/cm^2). In this case, the cyt *c* film was adsorbed from a much higher dissolved protein concentration (110 μM) and at lower ionic strength (7 mM) vs that used here (10 mM). In addition, Cheng's result was determined using a two-phase approximation[1] for the ATR experiment rather than the multilayer model employed here. Using the calculation procedure and data treatment described herein, we calculate a protein surface coverage from their data that is 13% lower (20 pmol/cm^2) than their published result. Clearly the use of different methods to calculate surface coverage does not fully explain the discrepancy between their surface coverage result and ours. Thus, we conclude that the higher dissolved protein concentration is probably the more important factor in accounting for the dicrepancy.

On ITO, the surface coverage is 21.7 ± 0.9 pmol/cm^2 (Table 2), which is close to a full monolayer of cyt *c*. Thus, although the conditions under which the cyt *c* was adsorbed to ITO and glass were identical in terms of protein concentration and ionic strength, the surface coverage is significantly higher than on glass. This shows that cyt *c* has a higher binding affinity for the ITO surface. A difference in binding affinities is not unexpected, since the surface chemistries of glass and ITO are significantly different. While there are protonated and deprotonated hydroxyls on both surfaces, ITO also has surface indium oxide and oxyhydroxide groups[29] that may have a stronger attraction for the charged amino acid groups (both positive and negative) on the surface of cyt *c*.

It is interesting to compare the spectroscopic surface coverage measurement on ITO (Table 2) to the electroactive surface coverage (measured by integrating the cathodic peak of a cyclic voltammogram of adsorbed cyt *c* on ITO). The electroactive surface coverage is only 9.5 pmol/cm^2, slightly less than a half monolayer,[18] which shows that less than half of the protein molecules adsorbed on the electrode surface can be directly oxidized or reduced. This could be due to the heterogeneous surface of ITO,[29] which has some insulating regions.[41] Another possibility is that a subpopulation of the adsorbed cyt *c* molecules is adsorbed in an orientation that places their heme groups too far from the surface to efficiently exchange electrons with the ITO surface. On the basis of our experience with different methods of forming electroactive cyt *c* films,[18,42] and the known heterogeneity of the ITO surface,[29,41] our hypothesis is that the properties of the ITO surface have a much greater effect on the electrochemistry of cyt *c* than the orientation of the adsorbed protein molecules.

Order Parameter, $\langle\cos^2\theta\rangle$. The dichroism of adsorbed cyt *c* films was quantified by determining one order parameter $\langle\cos^2\theta\rangle$ (or equivalently $\langle P_2(\cos\theta)\rangle = 3\langle\cos^2\theta\rangle/2 - {}^1/_2$).[43] By assuming that the heme in cyt *c* can be approximated as a circular dipole (D_{4h} symmetry),[44] for glass adsorbed cyt *c* films a value of $\langle\cos^2\theta\rangle = 0.30 \pm 0.02$ was calculated from eq 22, while on ITO substrates $\langle\cos^2\theta\rangle = 0.36 \pm 0.04$. Therefore, the first-order parameter is similar for films on both surfaces. Currently, we are combining these results with polarized fluorescence measurements on the Zn-substituted form of cyt *c*, which provides a second-order parameter, to enable a more thorough comparison of the molecular orientation distribution of these films. Results will be reported in a separate article.

5. Conclusions

In this paper, we have described the theory and application of the rigorous electromagnetic transfer-matrix approach for the calculation of anisotropic optical constants, surface coverage, and one order parameter in polarized ATR experiments. This approach can be used for any molecular film where the anisotropic complex refractive index can be described by eq 4. This method does not require the explicit calculation of the electric field across the absorbing layer, although it is implicitly and rigorously considered in the analysis.

To demonstrate the application of this approach, we have used it to calculate optical constants, surface coverage and one order parameter for adsorbed cyt *c* films on two different surfaces, glass and ITO. Although the films show no significant birefringence or dichroism and the order parameters are similar, the surface coverage of cyt *c* on glass is 0.5 monolayer, while on ITO the surface coverage is a full monolayer.

Acknowledgment. This work was funded by the National Science Foundation under Grant CHE-0108805 (to S.S.S.) and Grant DBI-0352449 (to S.B.M.). A.F.R. was partially supported by the Proposition 301 Graduate Fellowship in Photonics, University of Arizona and a Procter and Gamble student fellowship. N.C.R. was partially supported by the Undergraduate Biology Research Program, a training program at the University of Arizona that is funded by the Howard Hughes Medical Institute (52003749).

References and Notes

(1) Harrick, N. J. *Internal Reflection Spectroscopy*; Interscience Publishers: New York, 1967.

(2) Abeles. *Ann. Phys.* **1950**, *5*, 611.

(3) Hansen, W. N. *J. Opt. Soc. Am.* **1968**, *58*, 380.

(4) Picard, F.; Buffeteau, T.; Desbat, B.; Auger, M.; Pezolet, M. *Biophys. J.* **1999**, *76*, 539.

(5) Axelsen, P. H.; Citra, M. J. *Prog. Biophys. Mol. Biol.* **1996**, *66*, 227.

(6) Buffeteau, T.; Blaudez, D.; Pere, E.; Desbat, B. *J. Phys. Chem. B* **1999**, *103*, 5020.

(7) Berreman. *J. Opt. Soc. Am.* **1972**, *62*, 502.

(8) Yeh, P. *Optical Waves in Layered Media*; Wiley-Interscience: New York, 1988.

(9) Parikh, A. N.; Allara, D. L. *J. Chem. Phys.* **1992**, *96*, 927.

(10) Yamamoto, K.; Ishida, H. *Vib. Spec.* **1994**, *8*, 1.

(11) Sirkar, K.; Revzin, A.; Pishko, M. V. *Anal. Chem.* **2000**, *72*, 2930.

(12) Wilner, I.; Katz, E. *Angew. Chem., Int. Ed.* **2000**, *39*, 1180.

(13) Cheng, Y.-Y.; Lin, S. H.; Chang, H.-C.; Su, M.-C. *J. Phys. Chem. A* **2003**, *107*, 10687.

(14) Edmiston, P. L.; Lee, J. E.; Cheng, S.; Saavedra, S. S. *J. Am. Chem. Soc.* **1997**, *119*, 560.

(15) Murgida, D. H.; Hildebrandt, P. *Angew. Chem., Int. Ed.* **2001**, *40*, 728.

(16) Petralli-Mallow, T. P.; Plant, A. L.; Lewis, M. L.; Hicks, J. M. *Langmuir* **2000**, *16*, 5960.

(17) Boussaad, S.; Pean, J.; Tao, N. J. *Anal. Chem.* **2000**, *72*, 222.

(18) Runge, A. F.; Saavedra, S. S. *Langmuir* **2003**, *19*, 9418.

(19) Chen, X.; Ferrigno, R.; Yang, J.; Whitesides, G. M. *Langmuir* **2002**, *18*, 7009.

(20) El Kasmi, A.; Leopold, M. C.; Galligan, R.; Robertson, R. T.; Saavedra, S. S.; El Kacemi, K.; Bowden, E. F. *Electrochem. Commun.* **2002**, *4*, 177.

(21) Feng, Z. Q.; Imabayashi, S.; Kakiuchi, T.; Niki, K. *J. Chem. Soc., Faraday Trans.* **1997**, *93*, 1367.

(22) Mendes, S. B.; Saavedra, S. S. *Appl. Opt.* **2000**, *39*, 612.

(23) Mendes, S. B.; Li, L. F.; Burke, J. J.; Lee, J. E.; Saavedra, S. S. *Appl. Opt.* **1995**, *34*, 6180.

(24) Horowitz, F.; Mendes, S. B. *Appl. Opt.* **1994**, *33*, 2659.

(25) Macleod, H. A. *Thin-Film Optical Filters*; Macmillan: New York, 1986.

(26) Saleh, B. E. A.; Teich, M. C. *Fundamentals of Photonics*; John Wiley and Sons: New York, 1991.

(27) Mendes, S. B.; Bradshaw, J. T.; Saavedra, S. S. *Appl. Opt.* **2004**, *43*, 70.

(28) Brautigan, D. L.; Ferguson-Miller, S.; Margoliash, E. *Methods in Enzymology*; Fleischer, S., Packer, L., Eds.; Academic Press: New York City, 1978; Vol. 31−32; p 128.

(29) Donley, C.; Dunphy, D.; Paine, D.; Carter, C.; Nebesny, K.; Lee, P.; Alloway, D.; Armstrong, N. A. *Langmuir* **2002**, *18*, 450.

(30) Scholten, M.; van den Meerakker, J. E. A. M. *J. Electrochem. Soc.* **1993**, *140*, 471.

(31) van den Meerakker, J. E. A. M.; Baarslag, P. C.; Scholten, M. *J. Electrochem. Soc.* **1995**, *142*, 2321.

(32) Doherty, W. J.; Donley, C. L.; Armstrong, N. R.; Saavedra, S. S. *Appl. Spectrosc.* **2002**, *56*, 920.

(33) Margoliash, E.; Frohwirt, N. *Biochem. J.* **1959**, *71*, 570.

(34) Shukurova, R. M.; Yamshchikov, E. F. *Opt. Spectrosc.* **1972**, *33*, 633.

(35) Li, W. B.; Segre, P. N.; Gammon, R. W.; Sengers, J. V.; Lamvik, M. *J. Chem. Phys.* **1994**, *101*, 5058.

(36) Orem, D.; Mendes, S. B. Unpublished data.

(37) Dickerson, R.; Kopna, M.; Weinzierl, J.; Warnun, J.; Eisenberg, D.; Margoliash, E. *J. Biol. Chem.* **1967**, *242*, 3015.

(38) Thormahlen, I.; Straub, J.; Grigull, U. *J. Phys. Chem. Ref. Data* **1985**, *14*, 933.

(39) Kekicheff, P.; Laughlin, R. G.; Munyon, R. L. *Langmuir* **2001**, *17*, 4693.

(40) Lee, J. E.; Saavedra, S. S. *Langmuir* **1996**, *12*, 4025.

(41) Liau, Y.; Scherer, N. F.; Rhodes, K. *J. Phys. Chem. B* **2001**, *105*, 3282.

(42) Runge, A.; Mendes, S. B.; Saavedra, S. S. Manuscript in preparation.

(43) Bos, M. A.; Kleijn, J. M. *Biophys. J.* **1995**, *68*, 2566.

(44) Eaton, W. A.; Hochstrasser, R. M. *J. Chem. Phys.* **1967**, *46*, 2533.